Arabian Journal of Chemistry (2021) **14**, 102911

King Saud University

Arabian Journal of Chemistry

www.ksu.edu.sa
www.sciencedirect.com

ORIGINAL ARTICLE

A photo-induced electron transfer based reversible fluorescent chemosensor for specific detection of mercury (II) ions and its applications in logic gate, keypad lock and real samples

R. Kumar [a], **S. Ravi** [a,*], **C. Immanuel David** [b], **R. Nandhakumar** [b,*]

[a] *Department of Chemistry, Karpagam Academy of Higher Education, Eachanari, Coimbatore 641 021, India*
[b] *Department of Applied Chemistry, Karunya Institute of Technology and Sciences (Deemed-to-be University), Karunya Nagar, Coimbatore 641 114, India*

Received 23 September 2020; accepted 9 November 2020
Available online 17 November 2020

KEYWORDS

Fluorescence;
Rhodanine;
Chemosensor;
Mercury recognition;
Reversible;
Molecular mimicking

Abstract A quantitative mercuric detection is very important in the environmental and biological systems. In this paper, we report a novel bis-rhodanine derived fluorescent chemosensor for recognition of Hg^{2+} ion in DMSO-H_2O (1:1) medium. The 'turn-on' fluorescence response was exhibited specifically toward Hg^{2+} over other metal ions by receptor **R2** at 410 nm, which could be ascribed to the restriction of photo-induced electron transfer (PET) process and chelation-enhanced fluorescence (CHEF) effect upon the complexation with mercury ions. The complexing stoichiometry of receptor **R2** to Hg^{2+} was estimated to be 1:1 according to Job's plot experiments. The limit of detection was calculated to be 7.33×10^{-7} M based on the concentration dependent emission changes with good association constant of 8.97×10^{4} M^{-1}. As a result, we express that receptor **R2** is a promising candidate for Hg^{2+} recognition without any significant interference of other co-existing cations. The receptor **R2** was successfully applied to molecular logic and keypad lock applications and real water samples to determine its potential applications.

1. Introduction

Mercury (II) is the one of the largely dispensed toxic metal ions of any foreign species in the ecosystem and environment area (Renzoni et al., 1998; Benoit et al., 1998; Burg, 1995; Clarkson et al., 2003; Harada, 1995; Joshi et al., 2012). It has been widely employed for the different industrial objectives, considerably enlarging the feasibility of atmospheric pollution and the likelihood of human exposure (Zahir et al.,

* Corresponding authors.
E-mail addresses: ravisubban@rediffmail.com (S. Ravi), nandhakumar@karunya.edu (R. Nandhakumar).
Peer review under responsibility of King Saud University.

Production and hosting by Elsevier

https://doi.org/10.1016/j.arabjc.2020.11.017
1878-5352

2005., Grandjean et al., 1998; Matsumoto et al., 1965). Through the skin, respiratory or digestive system, mercury and its derivatives can invade living system and could create acute poisoning, respiratory tract infections, infectious pneumonia, chronic mercury poisoning, chronic mental illness, etc. (Nolan and Lippard, 2008; D'ltri et al., 1978; Czarnik, 1993; Kim et al., 2012; Behta and Ahmed, 2018). The Hg^{2+} accumulation can trigger cell dysfunction which eventually leads to miscellaneous health effects such as neurotoxicity, nephrotoxicity, hepatotoxicity, etc., in human and animal biological system due to the thiophilic nature of Hg^{2+} upon complexation with sulphur containing amino acids in proteins and enzymes (Silbergeld et al., 2005; Hoyle and Handy, 2005; Boening, 2000). In the 1950′s, the fatal Chisso-Minamata disease (a methylmercury poisoning) was caused by the daily consumption of fish and shell fish from the mercury contaminated waters (Ha et al., 2017; Eto et al., 2002; Mahaffey et al., 2004; Raju et al., 2020). Moreover, mercury pollution has become a global concern owing to its non-biodegradable and bioaccumulative character in the nature and living environment (Wang et al., 2020; Prabhu et al., 2014). According to the world health organization (WHO) report, the maximum permissible limit of Hg^{2+} in drinking water is 6 ppb (WHO., 2008). Therefore, the selective, reliable, and rapid recognition procedure for Hg^{2+} ions is of important challenge to the scientific and environmental bodies (Zhang et al., 2018; Jiang et al., 2018).

A variety of analytical techniques have been followed to determine the metal ion concentrations including, voltammetry, atomic absorption spectroscopy, plasma-atomic emission spectrometry, potentiometry, inductively coupled plasma mass spectroscopy, electrothermal atomic absorption spectroscopy, and fluorescence spectroscopy (Prabhu et al., 2019; Suresh et al., 2019; Lum and Leung, 2019; Feichtmeier and Leopold, 2014; Omidi et al., 2015; Bhuvanesh et al., 2018a, 2018b; Tan et al., 2012; Wygladacz et al., 2005; Liang et al., 2004; Chen and Zhu, 2005; Baron et al., 2000; Garcia et al., 2003; Singh and Pambid, 1990; Ndung'u et al., 2006; Yang and Sturgeon, 2002; Katarina et al., 2006; Bothra et al., 2017; Shamsipur et al., 2002). Unfortunately, fluorescent based chemosensors have captivated most of the researchers because of the accuracy in measurement, ease experimentation, rapid responses, and real-time monitoring in the practical area of recognition of metal ions (Li et al., 2018; Hu et al., 2016; Chen et al., 2019; Yang et al., 2015; Nandre et al., 2017; Goyal et al., 2010; Hu et al., 2020; Sahu et al., 2020). Despite, there are some limitations still occur in fluorescent based chemosensors such as tedious synthetic procedure, incapable detection in various solvent medium, turn-off response, longer detection time span, irreversible feature, and weak fluorescence in different pH ranges which predominantly influences the chemosensor applications (Ding et al., 2019; Huang et al., 2019; Liu et al., 2018; Ding et al., 2017). Under this context, developing a turn-on fluorescence responsive, profoundly sensitive and selective, cheap, and convenient fluorescent based chemosensor is vital.

Herein, we describe a novel fluorescent "turn-on" response chemosensor (**R2**) based on rhodanine derivative and 4-nitrobenzaldehyde synthesized via Knoevenagel condensation reaction as depicted in Scheme. 1. Rhodanine has significant number of heteroatoms (S, N, and O) in their structures which can chelate with metal ions very easily to provide some interesting electronic properties. These properties are helpful for the development of fluorescent based chemosensor for different analytes (Chen et al., 2016; Kundu et al., 2013). The sensing behavior of receptor (**R2**) was monitored by photoluminescence spectroscopy, surprisingly toward Hg^{2+} ion over other metal ions through photo-induced electron transfer (PET) and chelation-enhanced fluorescence (CHEF) mechanisms with the complete reversibility upon EDTA in DMSO-H_2O (1:1) medium. Accordingly, the reversibility fluorescence switching mechanism of receptor **R2** from Hg^{2+} using EDTA was utilized auspiciously to construct the potential molecular logic mimicking and keypad lock activities. Furthermore, the designed receptor **R2** has specific nature to scavenge the Hg^{2+} ions in DMSO-H_2O (1:1) medium without any disturbance of other cations and can be perturbed to detect trace amount of Hg^{2+} in real water samples.

2. Experimental section

2.1. Apparatus and materials

All reagents and solvents were purchased from commercial suppliers in analytical and spectroscopic grade used without any purification process. ^{1}H NMR and ^{13}C NMR spectra were obtained on Bruker Avance III 400 MHz and 100 MHz spectrometer with TMS as internal standard. UV–vis absorption spectra and fluorescence emission spectra were recorded on Jasco V-730 spectrophotometer and Jasco FP-8200 spectrophotometer at 24 ± 1 °C. A solution of metal ions was prepared from the chloride and nitrate salts of Ag^+, Al^{3+}, Ba^{2+}, Bi^{3+}, Ca^{2+}, Cd^{2+}, Co^{2+}, Cr^{3+}, Cu^{2+}, Fe^{2+}, Fe^{3+}, Hg^{2+}, K^+, Li^{2+}, Mg^{2+}, Mn^{2+}, Na^+, Ni^{2+}, Pb^{2+}, Sr^{2+}, Zn^{2+} and Zr^{2+} in DMSO-H_2O, 1:1 (v/v) HEPES buffered solution (50 mM) at pH = 7.4. The receptor **R2** was prepared in the concentration of 2×10^{-5} M and 2×10^{-6} M in DMSO-H_2O, 1:1 (v/v) HEPES buffered solution (50 mM) at pH = 7.4 for UV–vis absorption studies. And the concentration of receptor **R2** was 4×10^{-6} M in DMSO-H_2O, 1:1 (v/v) HEPES buffered solution (50 mM) at pH = 7.4 for overall the fluorescence spectral measurements.

2.2. Synthesis and characterization of receptor R2

The receptor **R2** was synthesized via a two-step process, as illustrated in Scheme. 1. 1,2-diamino propane (0.74 g, 0.01 mol) and carbon disulphide (1.52 g, 0.02 mol) were dissolved in the presence of NaOH (0.16 g, 0.04 mol) and sodium chloroacetate (2.4 g, 0.02 mol) and stirred at room temperature for 4 h to yield 3,3′-(propane-1,2-diyl)bis(2-thioxothiazolidin-4-one) or bis-rhodanine as intermediate (3.1 g). It was followed by the Knoevenagel condensation, where the intermediate bis-rhodanine (2.5 g, 0.01 mol) with p-nitro benzaldehyde (4 g, 0.025 mol) in presence of sodium acetate (0.85 g, 0.01 mol) and acetic acid (0.6 g, 0.01 mol) was stirred at room temperature for 6 h. The reaction mixture was then cooled, and the resulted precipitate was filtered and washed with water, dried and recrystallised (ethanol) to afford the corresponding product receptor **R2** as a yellow color solid in 65% yield. All the reaction conditions were optimized to afford a good yield. M. p.: 290 °C. ^{1}H NMR (400 MHz, $CDCl_3$, ppm): δ 1.15 (d, J = 6.8 Hz, 3H), 4.07 (d, 1H), 4.8 (d, 1H), 5.4 (m, 1H), 7.9

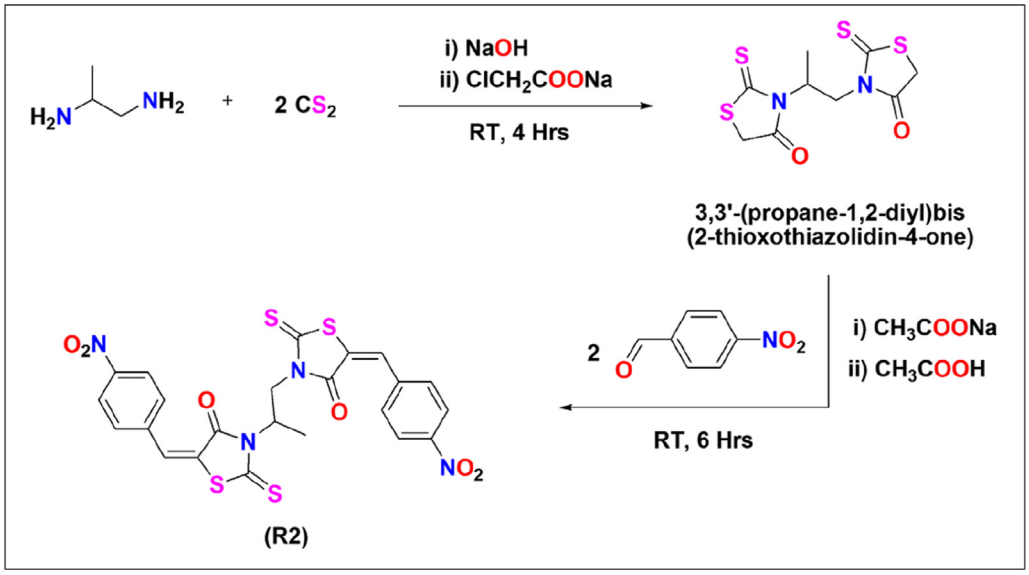

Scheme 1 Synthesis of receptor **R2.**

(m, 2H), 8.1 (m, 8H). ^{13}C NMR (100 MHz, DMSO, ppm): δ 203.3, 201.3, 174.87, 174.62, 151.14, 149.94, 145.7, 143.9, 134.7, 125.38, 51.02, 44.84 and 14.8. Elemental analysis: $C_{23}H_{16}N_4O_6S_4$; calcd.; C, 48.24; H, 2.82; N, 9.78. found.; C, 48.13; H, 2.92; N, 9.69. (Fig. S1 and S2)

3. Results and discussion

3.1. Fluorescence emission studies

The receptor **R2** was made completely soluble in DMSO-H_2O, 1:1 (v/v) HEPES buffered solution (50 mM) at pH = 7.4 for overall fluorescence emission studies. The excitation wavelength was fixed at 385 nm for the metal binding fluorescence emission studies, which was confirmed by the absorption spectrum of receptor **R2** at various concentrations in DMSO-H_2O, 1:1 (v/v) HEPES buffered solution (50 mM) at pH = 7.4 solution (Fig. S3). The fluorometric selectivity experiment was carried out using receptor **R2** for the recognition of various metal ions in DMSO-H_2O, 1:1 (v/v) HEPES buffer solution (50 mM, pH = 7.4) and excited at 385 nm. The miscellaneous metal ions such as Ag^+, Al^{3+}, Ba^{2+}, Bi^{3+}, Ca^{2+}, Cd^{2+}, Co^{2+}, Cr^{3+}, Cu^{2+}, Fe^{2+}, Fe^{3+}, Hg^{2+}, K^+, Li^{2+}, Mg^{2+}, Mn^{2+}, Na^+, Ni^{2+}, Pb^{2+}, Sr^{2+}, Zn^{2+} and Zr^{2+} were employed to investigate the sensing property of the synthesized receptor **R2**. The receptor **R2** (4×10^{-6} M) showed low or non-fluorescence emission above 400 nm (excited at 385 nm) (Fig. 1a). However, upon the addition of various metal ions to the receptor **R2** remarkably displayed excellent "turn-on" response toward only Hg^{2+} ions at 410 nm and the other co-existing metal ions didn't induce any significant changes in fluorescence emission nature (Fig. 1b). The selective experimental results clearly showed that the receptor **R2** can potentially detect Hg^{2+} ions with good selectivity. In addition, the sensing ability of the receptor **R2** utilizing UV–Vis spectroscopy (colorimetric studies) have also been studied in presence of various cations. The experimental results showed no considerable absorbance changes in DMSO-H_2O, 1:1 (v/v) HEPES buffer solution (50 mM, pH = 7.4) (Fig. S4).

3.2. Competition experiment studies

The specific detection of Hg^{2+} was subsequently performed using the receptor **R2** with the excess equivalents of other aggressive metal ions due to the importance in practical applications. To form the system **R2** + M^{n+}, various metal ion solutions (150 equivalents) were added to receptor **R2** (4×10^{-6} M) and then the system **R2** + M^{n+} + Hg^{2+} was formed by adding Hg^{2+} (4×10^{-6} M) into the mixture. As a result, the fluorescence emission intensity has not changed with any notable increment/decrement by all the other background metal ions (Fig. 2). The combined cross-contamination experimental outcomes, further openly explained that the receptor **R2** possesses great Hg^{2+} discriminating character in DMSO-H_2O, 1:1 (v/v) HEPES buffer solution (50 mM, pH = 7.4) with high specificity and interference-free Hg^{2+} chemosensor even in the presence of biologically and environmentally dominating metal cations.

3.3. The binding of receptor R2 with Hg^{2+}

A quantitative experimental study was investigated to understand the fluorescence detection properties of receptor **R2** to Hg^{2+} ions using fluorescence titration profiles. As shown in Fig. 3a, the emission intensity was gradually increased with the increasing concentration (0–100 equivalents) of Hg^{2+} at 410 nm (λ_{ex} = 385 nm). The fluorescence emission reached the maximum level, when the concentration of Hg^{2+} increased to five times higher than the concentration of receptor **R2**. Moreover, the fluorescence emission of receptor **R2** showed good linear relationship in the increasing addition of Hg^{2+}, as shown in Fig. 3b. The limit of detection (calculated using $3\delta/S$, where δ is the standard deviation of the blank measurements, and S is the slope of linear calibration curve, reported by previous report Immanuel David et al., 2020; Saravanan et al., 2019; Bhuvanesh et al., 2020; Tekuri et al., 2019) was calculated to be 7.33×10^{-7} M, which was lower than the many recently reported chemosensors (Table 1). From this characteristic linear relationship in different concentration of Hg^{2+}, the

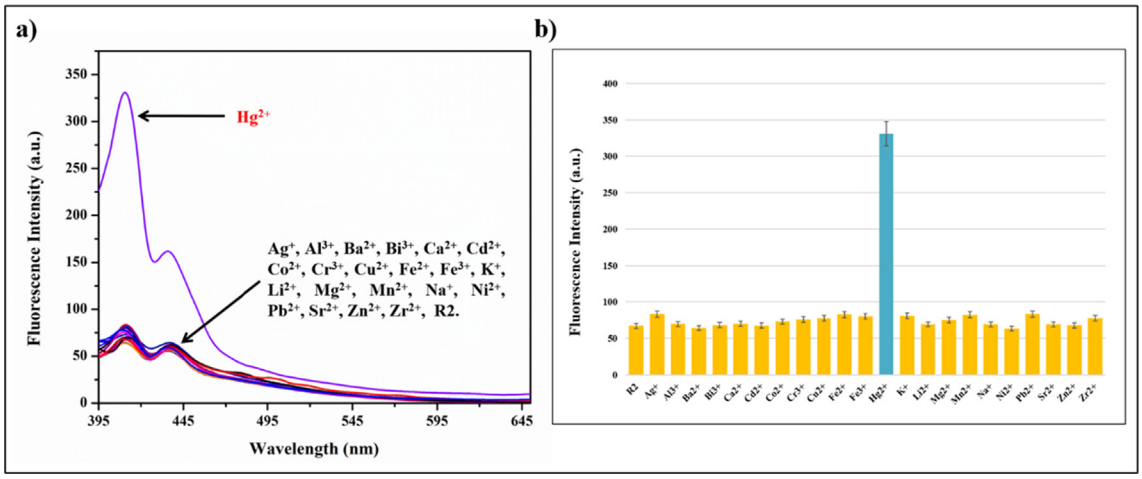

Fig. 1 a) Emission spectra of receptor **R2** (4×10^{-6} M) b) Emission response of receptor **R2** in DMSO-H_2O, 1:1 (v/v) HEPES buffer solution (50 mM, pH = 7.4) in the presence and absence of 100 equivalents of various metal ions at λ_{em} = 410 nm (λ_{ex} = 385 nm). Error bars indicate standard deviations (5%) from three repeated experiments.

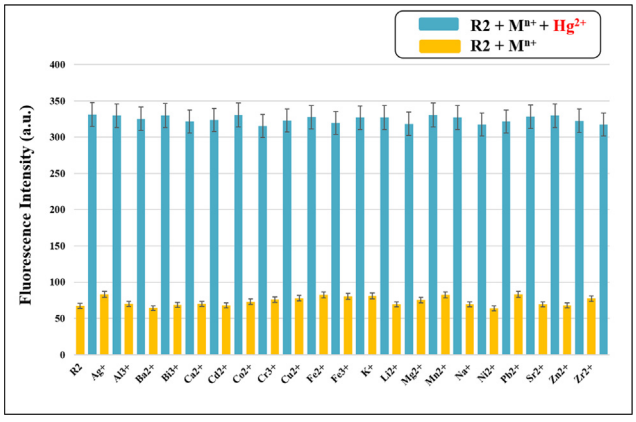

Fig. 2 Anti-interference studies of receptor **R2** (4×10^{-6} M) with Hg^{2+} ion and other metal ions (150 equivalents) in DMSO-H_2O, 1:1 (v/v) HEPES buffer solution (50 mM, pH = 7.4) at λ_{em} = 410 nm (λ_{ex} = 385 nm). Error bars indicate standard deviations (5%) from three repeated experiments.

receptor **R2** explore its potential to detect Hg^{2+} ions quantitatively. The remarkable fluorescence enhancement upon addition of Hg^{2+} into receptor **R2** was attributed to the binding of receptor **R2** with Hg^{2+} through restriction of photo induced electron transfer (PET) process causing the chelation-enhanced fluorescence (CHEF) effect, which results in the stronger emission in fluorescence spectrum.

Job's plot variation technique (Bhuvanesh et al., 2019; Velmurugan et al., 2018) was experimented to confirm the binding stoichiometric interaction of receptor **R2** + Hg^{2+} complex, which displayed maximum emission inflection point at 0.5 mol fraction. This clearly indicates that the coordination stoichiometry between receptor **R2** and Hg^{2+} is 1:1 formation as shown in Fig. 4. The binding constant (K_a) of receptor **R2** + Hg^{2+} complex was estimated to be 8.97×10^4 M^{-1} and R^2 value of 0.9849 by the Benesi-Hildebrand analysis (Velmurugan et al., 2020; Bhuvanesh et al., 2018a, 2018b) based on the fluorescence emission results (Fig. 5). The binding result designated the efficient binding of receptor **R2** with Hg^{2+} in DMSO-H_2O media.

3.4. Response of time and pH

The response time for the detection of Hg^{2+} by receptor **R2** in DMSO-H_2O, 1:1 (v/v) HEPES buffer solution (50 mM, pH = 7.4) was examined as illustrated in Fig. 6. It reveals that the fluorescence emission intensity of receptor **R2** attained the maximum influence upon binding of 100 equivalents of Hg^{2+} within 2.5 min and kept not fluctuate for 60 min. Therefore, the satisfactory outcome indicated that the receptor **R2** is highly stable and efficient for appropriate and rapid detection of Hg^{2+} ions in real sample testing. Moreover, to understand the photophysical properties of receptor **R2**, the effect of pH using fluorescence spectral measurements on receptor **R2** in absence and presence of Hg^{2+} ions were investigated in DMSO-H_2O, 1:1 (v/v) medium at 1.0–12.0 pH ranges (Fig. 7). Hydrochloric acid and Sodium hydroxide solutions were used to adjust the acidic and basic pH ranges. The receptor **R2** displays low and relatively stable fluorescence emission in acidic, basic and neutral pH ranges. Eventually, the low fluorescence was observed for **R2** + Hg^{2+} complex about 1.0 and 2.0 pH ranges. The emission gradually increased when basicity increases in the system and at the neutral point (7.0), the strongest emission was obtained. Afterwards, the system again started resuming toward weak fluorescence between the pH ranges of 9.0–12.0 due to the lack of stability in complexation. Based on the above pH effect results, the fluorescence detection of Hg^{2+} and further subjecting the biological assays could be supported by the receptor **R2** in a wide range of pH.

3.5. Reversibility of receptor R2 by EDTA

The reversibility of complexation of receptor **R2** toward Hg^{2+} was analysed by using chelating agent ethylene diamine tetra acetic acid (EDTA) as complexing ligand to determine the reusable property of receptor in the fluorescence detection. The

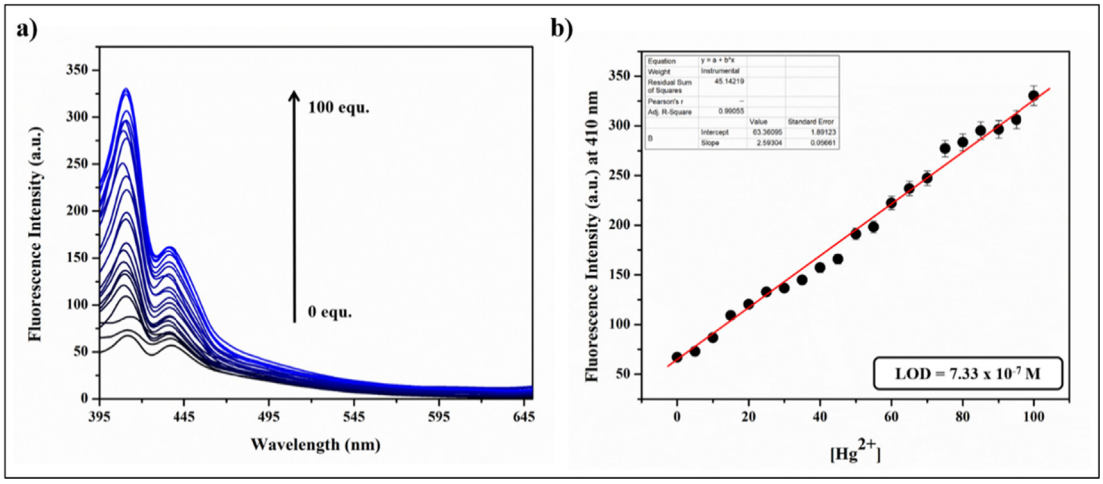

Fig. 3 a) Fluorescence emission spectra of receptor **R2** (4×10^{-6} M) upon addition of Hg^{2+} (0–100 equivalents) in DMSO-H_2O, 1:1 (v/v) HEPES buffer solution (50 mM, pH = 7.4) at λ_{em} = 410 nm (λ_{ex} = 385 nm) b) Calibration plot of fluorescence intensity vs concentration of Hg^{2+} at 410 nm upon gradual addition of Hg^{2+}. Error bars indicate standard deviations (5%) from three repeated experiments.

Table 1 Recent literature report on detection of Hg^{2+}.

Receptor type	Mode of detection	Testing media	Response time	K_a (M^{-1})	LOD (M)	Ref.
Perylene based	Turn-on	DMSO-H_2O (5:1)	1 min	–	0.35×10^{-6} M	Liu et al., 2020
Anthracene based	Turn-on	DMSO	–	5.35×10^{3} M^{-1}	6.34×10^{-6} M	Li et al., 2019
Quinoline based	Turn-on	Aqueous	–	6.56×10^{3} M^{-1}	1.01×10^{-6} M	Paisuwan et al., 2019
Naphthalimide based	Turn-off	MeCN- H_2O (4:1)	Less than a minute	3.76×10^{4} M^{-1}	0.83×10^{-6} M	Ye et al., 2019
Rhodanine based	Turn-on	MeCN- H_2O (9:1)	–	2.15×10^{4} M^{-1}	3.36×10^{-6} M	Bayindir (2019)
Rhodanine based	Turn-on	DMSO-H_2O (1:1)	2.5 min	8.97×10^{4} M^{-1}	7.33×10^{-7} M	This work

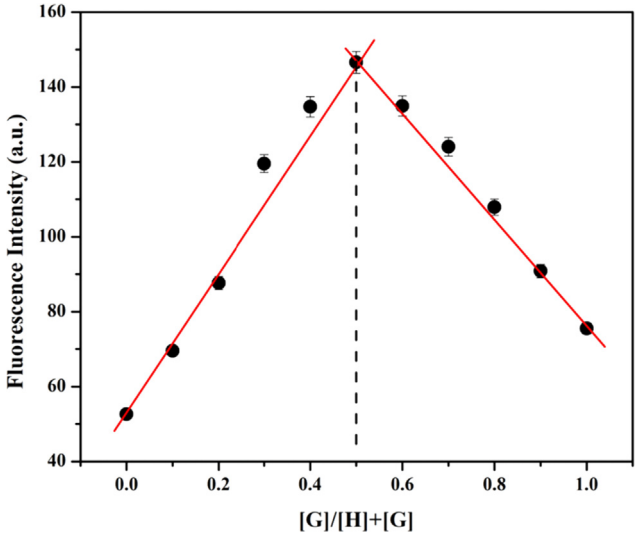

Fig. 4 Job's plot of the receptor **R2** + Hg^{2+} complex in DMSO-H_2O, 1:1 (v/v) HEPES buffer solution (50 mM, pH = 7.4) at λ_{em} = 410 nm (λ_{ex} = 385 nm). Error bars indicate standard deviations (5%) from three repeated experiments.

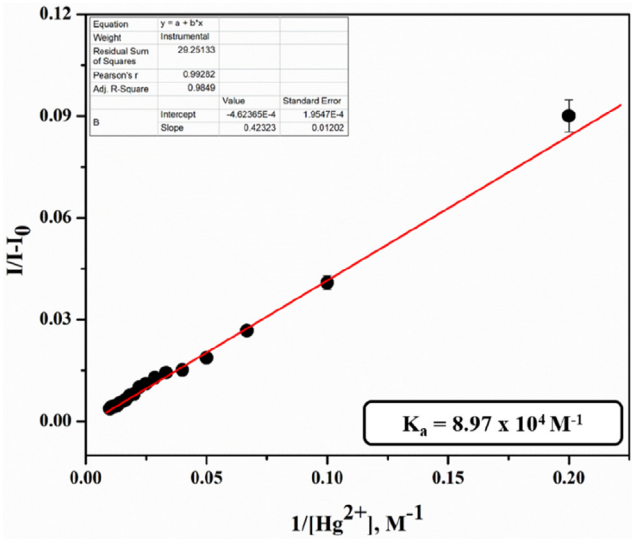

Fig. 5 Binding constant (K_a) of receptor **R2** with Hg^{2+} for 1:1 binding stoichiometry in DMSO-H_2O, 1:1 (v/v) HEPES buffer solution (50 mM, pH = 7.4) at λ_{em} = 410 nm (λ_{ex} = 385 nm). Error bars indicate standard deviations (5%) from three repeated experiments.

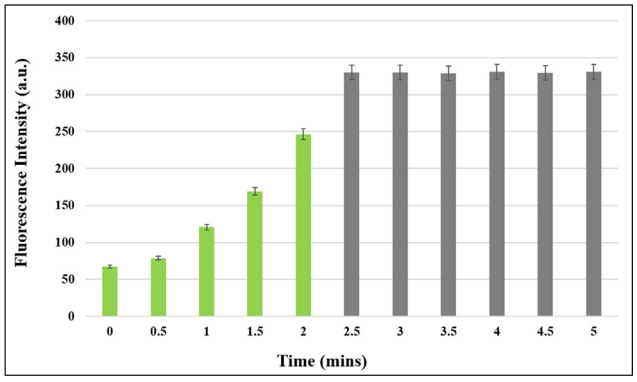

Fig. 6 The response time study of receptor **R2** to Hg^{2+}. Error bars indicate standard deviations (5%) from three repeated experiments.

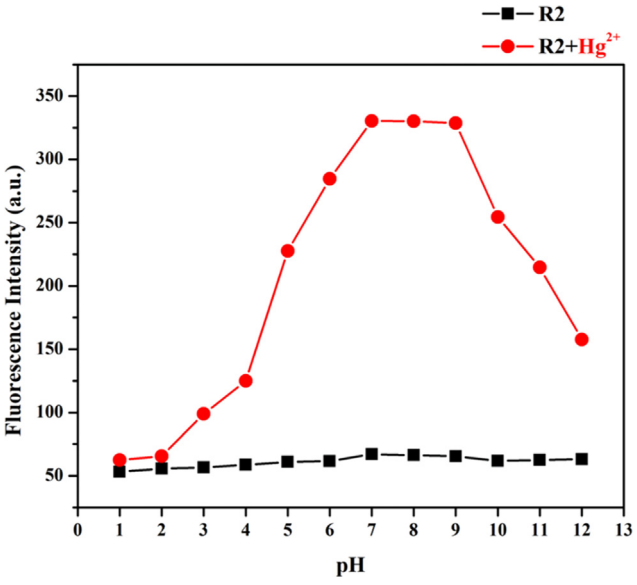

Fig. 7 The fluorescence emission changes of receptor **R2** in the absence and presence of Hg^{2+} at various pH ranges (1.0–12.0).

fluorescence emission disappeared and obtained very weak at 410 nm after the addition of EDTA to the receptor **R2** + Hg^{2+} complex solution in DMSO-H_2O, 1:1 (v/v) HEPES buffer solution (50 mM, pH = 7.4). This implied that the receptor **R2** was regenerated to its original position (fluorescence-off) from receptor **R2** + Hg^{2+} complex formation. In addition, the fluorescence intensity was recovered stronger (fluorescence-on) upon the addition of excess amount of Hg^{2+} into the **R2** + Hg^{2+} + EDTA mixture (Fig. 8a), and the combined results demonstrated that the reversible cycle could be unaffected for 5 more alternative additions of Hg^{2+} and EDTA (Fig. 8b). Hence, this reversible performance of receptor **R2** can be applied in the molecular logic gate construction.

3.6. Proposed sensing mechanism of receptor R2 to Hg^{2+}

On the basis of analytical and spectroscopic studies, a sensing mechanism of receptor **R2** to Hg^{2+} ion is proposed and shown in Scheme 2. The both carbonyl C═O groups of the receptor **R2** are involved in the complexation with Hg^{2+} ions. Therefore, the receptor **R2** acts as a fluorescence "Turn-off–on" sensor with respect to Hg^{2+}. The weak fluorescence of the receptor **R2** may be largely due to the photo-induced electron transfer (PET) process from the rhodanine moiety to phenyl derivative. Moreover, the receptor **R2** was freely movable along the side and unrestricted within the system in connection with C-C covalent linkage between two rhodanine moieties. Since, the absence of structural rigidity in the receptor molecule because of the intramolecular rotation, therein the charge transfer-excited singlet state is abruptly deactivated. However, the strong fluorescence exhibited upon the complexation of receptor **R2** with Hg^{2+} (1:1) due to the chelation-enhanced fluorescence (CHEF) effect, which resulted in the arrest of both PET process as well as C-C rotation that further increases the rigidity of the molecular assembly (Zhou et al., 2012; Maity and Govindaraju, 2011; Velmurugan et al., 2015; Mahajan et al., 2015). Additionally, the proposed coordination is also supported with Job's plot nonlinear curve fitting analysis with 1:1 complexing stoichiometry for receptor **R2** + Hg^{2+} complex. The color changes of the receptor **R2** in presence of various metal ions have been monitored by both naked eye and long UV–Vis (365 nm) light and are shown in Fig. S5.

3.7. Determination of fluorescence quantum yield

The fluorescence quantum yield (Φ) of the receptor **R2** and receptor **R2** + Hg^{2+} were derived based on the equation (Chae et al., 2019; Mittal et al., 2016)

$$\Phi_U = \Phi_R \times F_U/F_R \times A_R/A_U \times \eta U^2/\eta R^2$$

Here, F_U and F_R indicate the integrated fluorescence intensity of unknown and reference samples, respectively. A_U and A_R represent the absorbance of unknown and reference samples, respectively. ηU^2 (1.479) and ηR^2 (1.33) are refractive indexes of the solvents used to dissolve unknown and reference samples. Quinine sulphate (Φ = 0.54 in water) used as the reference for the measurement. The quantum yield (Φ) of receptor **R2** is 0.02, and for receptor **R2** + Hg^{2+} complex, it is found to be 0.26 at 410 nm.

3.8. IR spectral studies

The IR spectra of receptor **R2** and **R2** + Hg^{2+} complex was recorded separately. The receptor **R2** exhibits characteristic absorption bands at 1701 cm^{-1} ascribable to C═O stretching and 1195 cm^{-1} to C═S, respectively. The medium absorption band at 2376 cm^{-1} is due to the C—S stretching vibration. The strong absorptions at 1519 cm^{-1} (asym), 1257 cm^{-1} and 1323 cm^{-1} (sym) corresponding to N═O stretching. Upon addition of Hg^{2+} ion to the receptor **R2**, the absorption bands acquired at 1701 cm^{-1} is shifted to 1710 cm^{-1}, which indicates there is a possible coordination between the receptor **R2** and Hg^{2+} ions. (Fig. S6).

4. Applications

4.1. Molecular logic gate

The literature report says, the molecular logic function is the most conducting application and also has captivated great

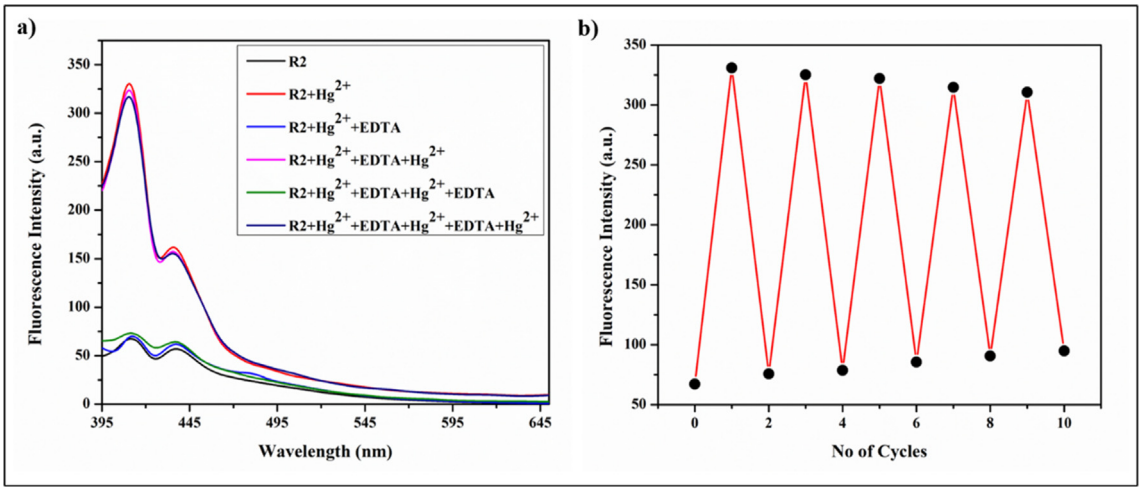

Fig. 8 a) Fluorescence emission spectra of reversibility of receptor **R2** experiment using EDTA b) Reversibility cycle upon alternative addition of Hg^{2+} and EDTA in DMSO-H_2O, 1:1 (v/v) HEPES buffer solution (50 mM, pH = 7.4) at λ_{em} = 410 nm (λ_{ex} = 385 nm).

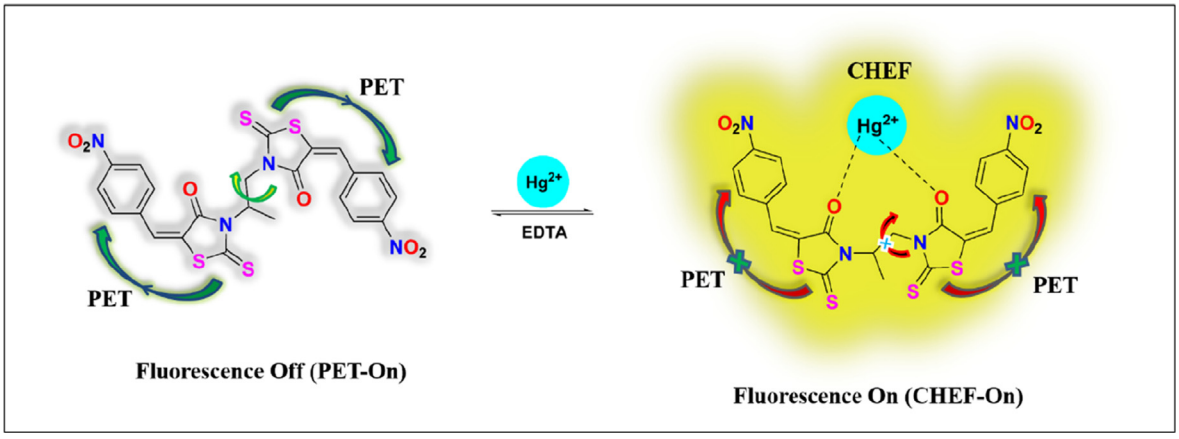

Scheme 2 Proposed sensing mechanism of receptor **R2** with Hg^{2+}.

attention among researchers (Erbas-Cakmak et al., 2018; Bai et al., 2020; Ma et al., 2019). The fluorescent reversible switching process of receptor **R2** was studied in molecular logic gate mimicking behavior. An INHIBIT logic gate could be built up based on the output of the reversible fluorescence signaling process in receptor **R2** + Hg^{2+} complex upon the addition of strong chelating agent EDTA. Therefore, the logic gate circuit was constructed by using Hg^{2+} and EDTA as two chemically encoded inputs and the fluorescence response at 410 nm as output (Fig. 9a). Based on the fluorescence spectroscopic data the truth table was constructed. The absence and presence of the chemical inputs (Hg^{2+} and EDTA) were considered as the binary code '0' and '1' respectively. For the output, the strong fluorescence was indicated as '1' or ON state and the weak fluorescence was indicated as '0' or OFF state during the signaling process (Fig. 9b). Based on the truth table the INHIBIT logic gate circuit was designed. In this system, the strong fluorescence '1' or ON state was generated in the output only with Hg^{2+} input alone (1,0). While all the other three input combinations were showed exceedingly weak fluorescence signals '0' or OFF state. Hence, the above results plainly proved the formation of INHIBIT logic gate for the robust reversible receptor **R2** (Fig. 9c).

4.2. Molecular keypad lock

The proposed molecular model can be used to construct sequence dependent molecular keypad lock based on the specific selectivity and excellent reversibility of receptor **R2**, Hg^{2+}, and EDTA. Here, receptor **R2**, Hg^{2+}, and EDTA as the three various chemical inputs and also labeled as 'R', 'H', and 'E' respectively. The probable six input combinations are RHE, REH, HRE, HER, ERH, and EHR. The combination RHE produced maximum fluorogenic output signal, whereas minimum output was unveiled by REH, HER, ERH, and EHR amidst these six input combinations (Fig. 10). Even though output HRE shows moderate fluorescence enhancement, it couldn't attain the complete "turn-on" mode to unlock the system. As an electronic keypad contains various keys (A-Z), the molecular keypad also restrains different keys and allows the accurate password (RHE) to unlock, wherein, all the other combinations are incorrect to open the locked system. For that

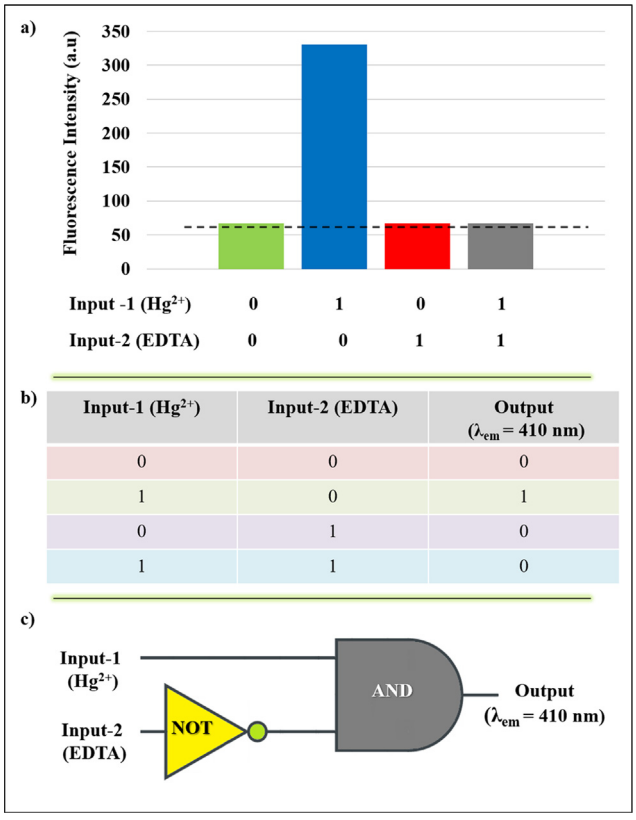

Fig. 9 a) Fluorescence intensity changes at 410 nm in presence four input combinations. b) Truth table for INHIBIT logic behavior. c) The INHIBIT molecular logic gate of receptor **R2**.

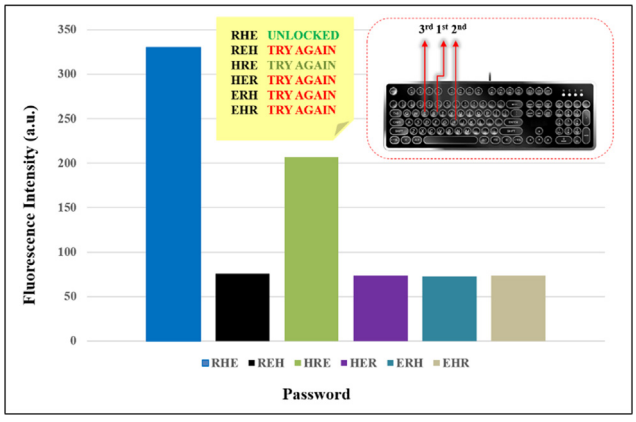

Fig. 10 Output for receptor **R2**, corresponding to probable six chemical input combinations at 410 nm. Inset: A molecular keypad lock triggering fluorescence emission at 410 nm when a correct password is entered, that is, RHE. The keys R, H, and E typify input receptor **R2**, Hg^{2+}, and EDTA, respectively.

reason, this type of sensing-based security systems may be accessible to keep the molecular level information safe (Wei et al., 2016; Vinoth Kumar et al., 2019).

Table 2 Detection of Hg^{2+} in real samples using receptor **R2.**

Sample	Hg^{2+} spiked (μM)	Hg^{2+} recovered (μM) mean[a] ± SD[b]	Recovery (%)	Relative error (%)
Tap water-1	5.0	4.85 ± 0.09	97.0	−3.0
Tap water-2	10.0	9.85 ± 0.04	98.5	−1.5
Drinking water-1	5.0	5.04 ± 0.03	100.8	0.8
Drinking water-2	10.0	9.48 ± 0.16	94.8	−5.2
Sewage water-1	5.0	4.92 ± 0.01	98.4	−1.6
Sewage water-2	10.0	9.81 ± 0.19	98.1	−1.9

[a] Mean of three measurement.
[b] Standard deviation.

4.3. Real sample detection

To investigate the practical applicability of the designed receptor **R2** for real sample detection, we evaluated the determination of Hg^{2+} ions in tap water, drinking water, and sewage water from different sources by using spike and recovery method. For this experiment, water samples were collected from Hepzibah Residence, KITS, Cbe, Tamil Nadu, India (Tap water); and Department of Applied Chemistry, KITS (Drinking water and sewage water). The test was conducted by spiking the known concentration of Hg^{2+} solution and calculating the recovery. The experimental results for the analytical measurements are given in Table 2. The obtained results were taken from each three repeated measurements in spiked real samples show massive recovery. Therefore, the results noticeably express the practical utility of the receptor **R2** for Hg^{2+} ion detection in real water samples.

5. Conclusion

In summary, we have developed a new fluorescent based chemosensor (**R2**) for the selective detection of Hg^{2+} ion over other metal ions with a 'turn-on' fluorescence response at 410 nm. The strong fluorescence enhancement noticed was due to the formation of chelation-enhanced fluorescence (CHEF) which blocks the photo-induced electron transfer (PET) process in receptor **R2** upon binding with Hg^{2+}. The experimental outcomes demonstrated the 1:1 binding stoichiometry for receptor **R2** + Hg^{2+} complex with low detection limit. Furthermore, the reversible switching process of receptor **R2** toward Hg^{2+} was examined by using EDTA with upto 10 cycles. Finally, based on these experimental results it is concluded that receptor **R2** can act as a highly selective and sensitive probe for detection of Hg^{2+} in logical mimicking and environmental monitoring works. The molecular logic and keypad lock applications along with the real water samples determination were demonstrated as the probe's applications. Further derivatives of the chemosensor **R2** for various other applications such as bioimaging, electrochemical detection along with their possible modes of binding using the Density Functional Theory studies are currently underway in our laboratory.

Acknowledgement

The authors gratefully thank the financial support of the SERB-EMR grant by the DST under sanction number *SERB-EMR/2016/005692*.

Declaration of Competing Interest

There are no conflicts of interest to declare.

Appendix A. Supplementary data

Supplementary data to this article can be found online at https://doi.org/10.1016/j.arabjc.2020.11.017.

References

Bai, L., Xu, Y., Li, L., Tao, F., Wang, S., Wang, L., Li, G., 2020. An efficient water-soluble fluorescent chemosensor based on furan Schiff base functionalized PEG for the sensitive detection of Al^{3+} in pure aqueous solution. New J. Chem. 44, 11148–11154.

Baron, M.G., Herrin, R.T., Armstrong, D.E., 2000. The measurement of silver in road salt by electrothermal atomic absorption spectrometry presented at SAC 99, Dublin, Ireland, July 25–30. Analyst. 125, 123–126.

Bayindir, S., 2019. A simple rhodanine-based fluorescent sensor for mercury and copper: The recognition of Hg^{2+} in aqueous solution, and Hg^{2+}/Cu^{2+} in organic solvent. J. Photochem. Photobiol. A. 372, 235–244.

Behta, M., Ahmed, N., 2018. Design and synthesis of 1,4-benzothiazine hydrazide as selective and sensitive colorimetric and turn-on fluorometric sensor for Hg^{2+} detection in aqueous medium. J. Photochem. Photobiol. A. 357, 41–48.

Benoit, J.M., Fitzgerald, W.F., Damman, A.W.H., 1998. The biogeochemistry of an ombrotrophic bog: Evaluation of use as an archive of atmospheric mercury deposition. Environ. Res. 78, 118–133.

Bhuvanesh, N., Suresh, S., Kannan, K., Rajesh Kannan, V., Maroli, N., Kolandaivel, P., Nandhakumar, R., 2019. Bis-anthracene derived bis-pyridine: selective fluorescence sensing of Al^{3+} ions. New J. Chem. 43, 2519–2528.

Bhuvanesh, N., Suresh, S., Prabhu, J., Kannan, K., Rajesh Kannan, V., Nandhakumar, R., 2018a. Ratiometric fluorescent chemosensor for silver ion and its bacterial cell imaging. Opt. Mater. 82, 123–129.

Bhuvanesh, N., Suresh, S., Ram Kumar, P., Mothi, E.M., Kannan, K., Rajesh Kannan, V., Nandhakumar, R., 2018b. Small molecule "turn on" fluorescent probe for silver ion and application to bioimaging. J. Photochem. Photobiol. A. 360, 6–12.

Bhuvanesh, N., Suresh, S., Velmurugan, K., Thamilselvan, A., Nandhakumar, R., 2020. Quinoline based probes: Large blue shifted fluorescent and electrochemical sensing of cerium ion and its biological applications. J. Photochem. Photobiol. A. 386, 112–120.

Boening, D.W., 2000. Ecological effects, transport, and fate of mercury: a general review. Chemosphere. 40, 1335–1351.

Bothra, S., Upadhyay, Y., Kumar, R., Ashok Kumar, S.K., Sahoo, S. K., 2017. Chemically modified cellulose strips with pyridoxal conjugated red fluorescent gold nanoclusters for nanomolar detection of mercuric ions. Biosens. Bioelectron. 90, 329–335.

Burg, R.V., 1995. Toxicology update. J. Appl. Toxicol. 15, 483–493.

Chae, J.B., Yun, D., Kim, S., Lee, H., Kim, M., Kim, K.-T., Kim, C., 2019. Fluorescent determination of zinc by a quinoline-based chemosensor in aqueous media and zebrafish. Spectrochim. Acta. A. 219, 74–82.

Chen, J.L., Zhu, C.Q., 2005. Functionalized cadmium sulfide quantum dots as fluorescence probe for silver ion determination. Anal. Chim. Acta. 546, 147–153.

Chen, J., Shu, W., Wang, E., 2016. A fluorescent and colorimetric probe based on isatin- appended rhodamine for the detection of Hg^{2+}. Chem. Res. Chin. Univ. 32, 742–745.

Chen, Z., Zhou, H., Gu, W., Liu, T., Xie, Z., Yang, L., Ma, L.J., 2019. A medium- controlled fluorescent enhancement probe for Ag^{+} and Cu^{2+} derived from pyrene- containing Schiff base. J. Photochem. Photobiol. A. 379, 5–10.

Clarkson, T.W., Magos, L., Myers, G.J., 2003. The toxicology of mercury-current exposures and clinical manifestations. N. Engl. J. Med. 349, 1731–1737.

Czarnik, A.W., 1993. Fluorescent chemosensors of ion and molecule recognition. American Chemical Society, Washington DC.

Ding, Y., Chen, M., Wu, K., Chen, M., Sun, L., Liu, Z., Shi, Z., Liu, Q., 2017. High- performance peroxidase mimics for rapid colorimetric detection of H_2O_2 and glucose derived from perylene diimides functionalized Co_3O_4 nanoparticles. Mater. Sci. Eng. C. 80, 558–565.

Ding, Y., Liu, H., Gao, L.N., Fu, M., Luo, X., Zhang, X., Liu, Q., Zeng, R.C., 2019. Fe-doped Ag_2S with excellent peroxidase-like activity for colorimetric determination of H_2O_2. J. Alloys Compd. 785, 1189–1197.

D'ltri, P.A., D'ltri, F.M., 1978. Mercury contamination: A human tragedy. Environ. Manage. 2, 3–16.

Erbas-Cakmak, S., Kolemen, S., Sedgwick, A.C., Gunnlaugsson, T., James, T.D., Yoon, J., Akkaya, E.U., 2018. Molecular logic gates: the past, present and future. Chem. Soc. Rev. 47, 2228–2248.

Eto, K., Tokunaga, H., Nagashima, K., Takeuchi, T., 2002. An autopsy case of Minamata disease (Methylmercury poisoning)-Pathological viewpoints of peripheral nerves. Toxicol. Pathol. 30, 714–722.

Feichtmeier, N.S., Leopold, K., 2014. Detection of silver nanoparticles in parsley by solid sampling high-resolution-continuum source atomic absorption spectrometry. Anal. Bioanal. Chem. 406, 3887–3894.

Garcia, I.L., Campillo, N., Arnau-Jerez, I., Hernandez-Cordoba, M., 2003. Slurry sampling for the determination of silver and gold in soils and sediments using electrothermal atomic absorption spectrometry. Spectrochim. Acta Part B. 58, 1715–1721.

Goyal, R.N., Gupta, V.K., Chatterjee, S., 2010. Voltammetric biosensors for the determination of paracetamol at carbon nanotube modified pyrolytic graphite electrode. Sens. Actuat. B Chem. 149, 252–258.

Grandjean, P., Weihe, P., White, R.F., Debes, F., 1998. Cognitive performance of children prenatally exposed to "Safe" levels of methylmercury. Environ Res. 77, 165–172.

Ha, E., Basu, N., Bose-O'Reilly, S., Dorea, J.G., McSorley, E., Sakamoto, M., Chan, H.M., 2017. Current progress on understanding the impact of mercury on human health. Environ. Res. 152, 419–433.

Harada, M., 1995. Minamata disease: methylmercury poisoning in Japan caused by environmental pollution. Crit. Rev. Toxicol. 25, 1–24.

Hoyle, I., Handy, R.D., 2005. Dose-dependent inorganic mercury absorption by isolated perfused intestine of rainbow trout, Oncorhynchus mykiss, involves both amiloride- sensitive and energy-dependent pathways. Aquat. Toxicol. 72, 147–159.

Huang, L., Yang, Z., Zhou, Z., Li, Y., Tang, S., Xiao, W., Hu, M., Peng, C., Chen, Y., Gu, B., Li, H., 2019. A dual colorimetric and near-infrared fluorescent turn-on probe for Hg^{2+} detection and its applications. Dyes Pigm. 163, 118–125.

Hu, J-P., He, J-X., Fang, H., Yang, H-H., Zhang, Q., Lin, Q., Yao, H., Zhang, Y-M., Wei, T- B., Qu, W-J., 2020. A novel pillar[5]arene-based emission enhanced supramolecular sensor for dual-channel selective detection and separation of Hg2+. New J. Chem. 44, 13157–13162.

Hu, Y., Wang, J., Long, L., Xiao, X., 2016. A ratiometric fluorescence sensor for Fe(3+) based on FRET and PET processes. Luminescence. 31, 16–21.

Immanuel David, C., Bhuvanesh, N., Haritha Jayaraj., Thamilselvan, A., Parimala devi, D., Abiram, A., Prabhu, J., Nandhakumar, R., 2020. Experimental and theoretical studies on a simple S−S-bridged dimeric Schiff base: Selective chromo-fluorogenic chemosensor for nanomolar detection of Fe2+ & Al3+ ions and its varied applications. ACS Omega. 5, 3055–3072.

Jiang, X.-M., Huang, X.-J., Song, S.-S., Ma, X.-Q., Zhang, Y.-M., Yao, H., Wei, T.-B., Lin, Q., 2018. Tri-pillar[5]arene-based multi-stimuli responsive supramolecular polymer for fluorescent detection and separation of Hg^{2+}. Polym. Chem. 9, 4625–4630.

Joshi, D., Mittal, D.K., Shukla, S., Srivastav, A.K., 2012. Therapeutic potential of N-acetyl cysteine with antioxidants (Zn and Se) supplementation against dimethylmercury toxicity in male albino rats. Exp. Toxicol. Pathol. 64, 103–108.

Katarina, R.K., Takayanagi, T., Oshima, M., Motomizu, S., 2006. Synthesis of a chitosan- based chelating resin and its application to the selective concentration and ultratrace determination of silver in environmental water samples. Anal. Chim. Acta. 558, 246–253.

Kim, H.N., Ren, W.X., Kim, J.S., Yoon, J., 2012. Fluorescent and colorimetric sensors for detection of lead, cadmium, and mercury ions. Chem. Soc. Rev. 41, 3210–3244.

Kundu, A., Pathak, S., Pramanik, A., 2013. Synthesis and fluorescence properties of isatin- based spiro compounds: Switch off chemosensing of copper(II) ions. Asian J. Org. Chem. 2, 869–876.

Liang, J.G., Ai, X.P., He, Z.K., Pang, D.W., 2004. Functionalized CdSe quantum dots as selective silver ion chemodosimeter. Analyst. 129, 619–622.

Li, J.B., Liu, Y., Zheng, X.Y., Wang, D., 2019. An off-on chemosensor for Hg^{2+} based on the excimer emission of anthracene. Microchem. J. 150, 104–108.

Liu, H., Ding, Y.N., Yang, B., Liu, Z., Zhang, X., Liu, Q., 2018. Iron doped $CuSn(OH)_6$ microspheres as a peroxidase-mimicking artificial enzyme for H_2O_2 colorimetric detection. ACS Sustain. Chem. Eng. 6, 14383–14393.

Liu, Y., Yang, L., Li, L., Liang, X., Li, S., Fu, Y., 2020. A dual thiourea-appended perylenebisimide "turn-on" fluorescent chemosensor with high selectivity and sensitivity for Hg^{2+} in living cells. Spectrochim. Acta A. 241, 118–127.

Li, Z.M., Hu, D., Wei, J., Qi, Q., Cao, X.P., Chow, H.F., Kuck, D., 2018. An efficient Ag^{+}-selective fluorescent chemosensor derived from tribenzotriquinacene. Synth. 50, 1457–1461.

Lum, J.T., Leung, K.S., 2019. Quantifying silver nanoparticle association and elemental content in single cells using dual mass mode in quadrupole-based inductively coupled plasma-mass spectrometry. Anal. Chim. Acta. 1061, 50–59.

Mahaffey, K.R., Clickner, R.P., Bodurow, C.C., 2004. Blood organic mercury and dietary mercury intake: National Health and Nutrition Examination Survey, 1999 and 2000. Environ. Health Perspect. 112, 562–570.

Mahajan, D., Khairnar, N., Bondhopadhyay, B., Sahoo, S.K., Basu, A., Singh, J., Singh, N., Bendre, R., Kuwar, A., 2015. A highly selective fluorescent 'turn-on' chemosensor for Hg^{2+} based on a phthalazin-hydrazone derivative and its application in human cervical cancer cell imaging. New J. Chem. 39, 3071–3076.

Maity, D., Govindaraju, T., 2011. Naphthaldehyde-Urea/Thiourea conjugates as turn-on fluorescent probes for Al^{3+} based on restricted C=N isomerization. Eur. J. Inorg. Chem. 36, 5479–5485.

Matsumoto, H., Koya, G., Takeuchi, T., 1965. Fetal minamata disease: A neuropathological study of two cases of intrauterine intoxication by a methyl mercury compound. J. Neuropathol. Exp. Neurol. 24, 563–574.

Ma, X.-Q., Wang, Y., Wei, T.-B., Qi, L.-H., Jiang, X.-M., Ding, J.-D., Zhu, W.-B., Yao, H., Zhang, Y.-M., Lin, Q., 2019. A novel AIE chemosensor based on quinoline functionalized Pillar[5]arene for highly selective and sensitive sequential detection of toxic Hg^{2+} and CN^{-}. Dyes Pigm. 164, 279–286.

Mittal, M., Jana, A., Sarkar, S., Priya, M., Sapra, S., 2016. Size of the organic cation tunes the band gap of colloidal organo lead bromide perovskite nanocrystals. J. Phys. Chem. 7, 3270–3277.

Nandre, J.P., Patil, S.R., Sahoo, S.K., Pradeep, C.P., Churakov, A., Yu, F., Chen, L., Redshaw, C., Patil, A.A., Patil, U.D., 2017. A chemosensor for micro- to nano-molar detection of Ag^{+} and Hg^{2+} ions in pure aqueous media and its applications in cell imaging. Dalton Trans. 46, 14201–14209.

Ndung'u, K., Ranville, M.A., Franks, R.P., Flegal, A.R., 2006. On-line determination of silver in natural waters by inductively-coupled plasma mass spectrometry: Influence of organic matter. Mar. Chem. 98, 109–120.

Nolan, E.M., Lippard, S.J., 2008. Tools and tactics for the optical detection of mercuric ion. Chem. Rev. 108, 3443–3480.

Omidi, F., Behbahani, M., Shahtaheri, S.J., Salimi, S., 2015. Trace monitoring of silver ions in food and water samples by flame atomic absorption spectrophotometry after preconcentration with solvent-assisted dispersive solid phase extraction. Environ. Monit. Assess. 187, 361–370.

Prabhu, J., Velmurugan, K., Nandhakumar, R., 2014. A highly selective and sensitive naphthalene-based chemodosimeter for Hg^{2+} ions. J. Lumin. 145, 733–736.

Prabhu, J., Velmurugan, K., Raman, A., Duraipandy, N., Kiran, M. S., Easwaramoorthi, S., Tang, L., Nandhakumar, R., 2019. Pyrene-phenylglycinol linked reversible ratiometric fluorescent chemosensor for the detection of aluminium in nanomolar range and its bio-imaging. Anal. Chim. Acta. 1090, 114–124.

Paisuwan, W., Rashatasakhon, P., Ruangpornvisuti, V., Sukwattanasinitt, M., Ajavakom, A., 2019. Dipicolylamino quinoline derivative as novel dual fluorescent detecting system for Hg^{2+} and Fe^{3+}. Sens. Biosensing. Res. 24, 100–109.

Raju, V., Selvakumar, R., Ashok kumar, S.K., Madhu, G., Bothra, S., Sahoo, S.K., 2020. A ninhydrin-thiosemicarbazone based highly selective and sensitive chromogenic sensor for Hg2+ and F- ions. J. Chem. Sci. 132, 89.

Renzoni, A., Zino, F., Franchi, E., 1998. Mercury levels along the food chain and risk for exposed populations. Environ. Res. 77, 68–72.

Sahu, M., Manna, A.K., Rout, K., Mondal, J., Patra, G.K., 2020. A highly selective thiosemicarbazone based Schiff base chemosensor for colorimetric detection of Cu^{2+} and Ag^{+} ions and turn-on fluorometric detection of Ag^{+} ions. Inorganica Chim. Acta. 508, 119–127.

Saravanan, A., Shyamsivappan, S., Suresh, T., Subashini, G., Kadirvelu, K., Bhuvanesh, N., Nandhakumar, R., Mohan, P.S., 2019. An efficient new dual fluorescent pyrene based chemosensor for the detection of bismuth (III) and aluminium (III) ions and its applications in bio-imaging. Talanta. 198, 249–256.

Shamsipur, M., Javanbakht, M., Lippolis, V., Garau, A., Filippo, G. D., Ganjali, M.R., Yari, 2002. A. Novel Ag+ ion-selective electrodes based on two new mixed azathioether crowns containing a 1,10-phenanthroline sub-unit. Anal. Chim. Acta. 462, 225–234.

Silbergeld, E.K., Silva, I.A., Nyland, J.F., 2005. Mercury and autoimmunity: implications for occupational and environmental health. Toxicol. Appl. Pharmacol. 207, 282–292.

Singh, R.P., Pambid, E.R., 1990. Selective separation of silver from waste solutions on chromium(III) hexacyanoferrate(III) ion exchanger. Analyst. 115, 301–304.

Suresh, S., Bhuvanesh, N., Raman, A., Sugumar, P., Padmanabhan, D., Easwaramoorthi, S., Ponnuswamy, N.M., Kavitha, S., Nandhakumar, R., 2019. Experimental and theoretical studies of imidazole based chemosensor for Palladium and their biological applications. J. Photochem. Photobiol. A. 385, 112–121.

Tan, E., Yin, P., Lang, X., Wang, X., You, T., Guo, L., 2012. Functionalized gold nanoparticles as nanosensor for sensitive and selective detection of silver ions and silver nanoparticles by surface-enhanced Raman scattering. Analyst. 137, 3925–3928.

Tekuri, V., Sahoo, S.K., Trivedi, D.R., 2019. Hg^{2+} induced hydrolysis of thiazole amine based Schiff base: Colorimetric and fluorogenic chemodosimeter for Hg^{2+} ions in an aqueous medium. Spectrochim. Acta A. 218, 19–26.

Velmurugan, K., Mathankumar, S., Santhoshkumar, S., Amudha, S., Nandhakumar, R., 2015. Specific fluorescent sensing of aluminium using naphthalene benzimidazole derivative in aqueous media. Spectrochim. Acta A. 139, 119–123.

Velmurugan, K., Prabhu, J., Raman, A., Duraipandy, N., Kiran, M. S., Easwaramoorthi, S., 2018. Dual functional fluorescent chemosensor for discriminative detection of Ni^{2+} and Al^{3+}-ions and its imaging in living cells. ACS Sustain. Chem. Eng. 6, 16532–16543.

Velmurugan, K., Vickram, R., Karthick, R., Jipsa, C.V., Suresh, S., Prabakaran, G., Prabhu, J., Velraj, G., Nandhakumar, R., 2020. Binol diuryl dipyrene fluorescent probe: dual detection of silver and carbonate ions and its bioimaging applications. J. Photochem. Photobiol. A. 401, 112–123.

Vinoth Kumar, G.G., Kannan, R.S., Yang, T.C., Rajesh, J., Sivaraman, G., 2019. An efficient "Ratiometric" fluorescent chemosensor for the selective detection of Hg^{2+} ions based on phosphonates: its live cell imaging and molecular keypad lock applications. Anal. Methods. 11, 901–916.

Wang, J.H., Liu, Y.M., Dong, Z.M., Chao, J.B., Wang, H., Wang, Y., Shuang, S.J., 2020. New colorimetric and fluorometric chemosensor for selective Hg^{2+} sensing in a near- perfect aqueous solution and bio-imaging. Hazard. Mater. 382, 121–130.

Wei, T.B., Li, W.T., Li, Q., Qu, W.J., Li, H., Yan, G.T., Lin, Q., Yao, H., Zhang, Y.M., 2016. A dual-channel chemosensor could successively detect CN^- and HSO_4^- in an aqueous solution and act as a keypad lock. RSC Adv. 6, 43832–43837.

Who guidelines values for chemicals that are of health significance in drinking water, Guidelines for drinking water quality, 3rd Edn. (2008).

Wygladacz, K., Radu, A., Xu, C., Qin, Y., Bakker, E., 2005. Fiber-Optic microsensor array based on fluorescent bulk optode microspheres for the trace analysis of silver ions. Anal. Chem. 77, 4706–4712.

Yang, L., Sturgeon, R.E., 2002. On-line determination of silver in seawater and marine sediment by inductively coupled plasma mass spectrometry. J. Anal. At. Spectrom. 17, 88–93.

Yang, Z., She, M., Yin, B., Hao, L., Obst, M., Liu, P., Li, J., 2015. Solvent-dependent turn-on probe for dual monitoring of Ag^+ and Zn^{2+} in living biological samples. Anal. Chim. Acta. 868, 53–59.

Ye, F., Liang, X.M., Xu, K.X., Pang, X.X., Chai, Q., Fu, Y., 2019. A novel dithiourea- appended naphthalimide "on-off" fluorescent probe for detecting Hg^{2+} and Ag^+ and its application in cell imaging. Talanta. 200, 494–502.

Zahir, F., Rizwi, S.J., Haq, S.K., Khan, R.H., 2005. Low dose mercury toxicity and human health. Environ. Toxicol. Pharmacol. 20, 351–360.

Zhang, Y.-M., Zhu, W., Huang, X.-J., Qu, W.-J., He, J.-X., Fang, H., Yao, H., Wei, T.-B., Lin, Q., 2018. Supramolecular Aggregation-Induced Emission gels based on pillar[5]arene for ultrasensitive detection and separation of multianalytes. ACS Sustain. Chem. Eng. 6, 16597–16606.

Zhou, X., Li, P., Shi, Z., Tang, X., Chen, C., Liu, W., 2012. A highly selective fluorescent sensor for distinguishing cadmium from zinc ions based on a quinoline platform. Inorg. Chem. 51, 9226–9231.